Structural basis for the cooperative interplay between the two causative gene products of combined factor V and factor VIII deficiency

Miho Nishio[a,b,c], Yukiko Kamiya[a,b,c], Tsunehiro Mizushima[a], Soichi Wakatsuki[d], Hiroaki Sasakawa[c], Kazuo Yamamoto[e], Susumu Uchiyama[f], Masanori Noda[f], Adam R. McKay[g], Kiichi Fukui[f], Hans-Peter Hauri[h], and Koichi Kato[a,b,c,i,j,1]

[a]Department of Structural Biology and Biomolecular Engineering, Graduate School of Pharmaceutical Sciences, Nagoya City University, 3-1 Tanabe-dori, Mizuho-ku, Nagoya 467-8603, Japan; [b]Okazaki Institute for Integrative Bioscience and [c]Institute for Molecular Science, National Institutes of Natural Sciences, 5-1 Higashiyama, Myodaiji, Okazaki 444-8787, Japan; [d]Structural Biology Research Center, Photon Factory, Institute of Materials Structure Science, High Energy Accelerator Research Organization (KEK), Tsukuba, Ibaraki 305-0801, Japan; [e]Graduate School of Frontier Sciences, University of Tokyo, 5-1-5 Kashiwanoha, Kashiwa, Chiba 277-8562, Japan; [f]Department of Biotechnology, Graduate School of Engineering, Osaka University, 2-1 Yamadaoka, Suita, Osaka 565-0871, Japan; [g]Department of Chemistry, University College London, 20 Gordon Street, London WC1H 0AJ, United Kingdom; [h]Biozentrum, University of Basel, 50-70 Klingelbergstrasse CH-4056 Basel, Switzerland; [i]The Glycoscience Institute, Ochanomizu University, 2-1-1 Ohtsuka, Bunkyo-ku, Tokyo 112-8610, Japan; and [j]GLYENCE Co., Ltd., 2-22-8 Chikusa, Chikusa-ku, Nagoya 464-0858, Japan

Edited by Jonathan S. Weissman, University of California, San Francisco, CA, and approved December 22, 2009 (received for review July 29, 2009)

Combined deficiency of coagulation factors V and VIII (F5F8D), an autosomal recessive disorder characterized by coordinate reduction in the plasma levels of factor V (FV) and factor VIII (FVIII), is genetically linked to mutations in the transmembrane lectin ERGIC-53 and the soluble calcium-binding protein MCFD2. Growing evidence indicates that these two proteins form a complex recycling between the endoplasmic reticulum (ER) and the ER-Golgi intermediate compartment and thereby function as a cargo receptor in the early secretory pathway of FV and FVIII. For better understanding of the mechanisms underlying the functional coordination of ERGIC-53 and MCFD2, we herein characterize their interaction by x-ray crystallographic analysis in conjunction with NMR and ultracentrifugation analyses. Inspection of the combined data reveals that ERGIC-53-CRD binds MCFD2 through its molecular surface remote from the sugar-binding site, giving rise to a 1:1 complex in solution. The interaction is independent of sugar-binding of ERGIC-53 and involves most of the missense mutation sites of MCFD2 so far reported in F5F8D. Comparison with the previously reported uncomplexed structure of each protein indicates that MCFD2 but not ERGIC-53-CRD undergoes significant conformational alterations upon complex formation. Our findings provide a structural basis for the cooperative interplay between ERGIC-53 and MCFD2 in capturing FV and FVIII.

MCFD2 | ERGIC-53 | calcium-binding protein | cargo receptor | intracellular lectin

Combined deficiency of coagulation factors V and VIII (F5F8D) is an autosomal recessive disorder characterized by coordinate reduction in the plasma levels of factor V (FV) and factor VIII (FVIII) (1, 2) Extensive genetic analysis of F5F8D patients identified two genes that are associated with this disorder. Genetic mutations in *LMAN1* account for approximately 70% of F5F8D families, whereas the remaining 30% families possess mutation in *MCFD2* (3, 4). *LMAN1* encodes the transmembrane lectin ERGIC-53 (ER-Golgi intermediate compound protein of 53 kDa) (5), which possesses a luminal carbohydrate recognition domain (CRD) with specificity for high-mannose-type oligosaccharides (6, 7) and forms dimers or hexamers stabilized by disulfide bonds formed in its stalk domain (5, 8). By contrast, the product of *MCFD2* is a soluble luminal protein with two EF-hand Ca^{2+}-binding motifs (9). It has been shown that MCFD2 interacts with the CRD of ERGIC-53 in a Ca^{2+}-dependent manner (9–11). Accumulating evidence indicates that this complex recycles between the endoplasmic reticulum (ER) and the ER-Golgi intermediate compartment (ERGIC) and thereby functions as a cargo receptor in the early secretory pathway of FV and FVIII (12).

To gain a better understanding of the molecular mechanisms underlying the sorting and trafficking of these coagulation factors, it is essential to shed light on the structural basis of the cooperative interplay between ERGIC-53 and MCFD2. The crystallographic data of the CRD of rat ERGIC-53 have revealed that it comprises one concave and one convex β-sheet packed into a β-sandwich with structural resemblance to leguminous lectins (13, 14). Although a highly homologous CRD is shared by VIP36 (15), which is a cargo receptor putatively involved in the retrograde transport of glycoproteins from the Golgi to the ER (6, 16), this lectin is not capable of interacting with MCFD2 (10). Three-dimensional structure of MCFD2 has been determined by NMR spectroscopy (17). In the presence of Ca^{2+} ions, MCFD2 adopts a calmodulin-like EF-hand domain composed of four α-helices, leaving the N-terminal 68 residues unstructured. However, the mode of interaction between ERGIC-53 and MCFD2 remains largely unknown.

In the present study, we present the three-dimensional structure of MCFD2 and the CRD of ERGIC-53 determined by x-ray crystallographic analysis in conjunction with NMR and ultracentrifugation studies. These data provide a structural basis of the functional coordination of the two causative gene products for F5F8D.

Results

Overall Structure of the Complex. The structure of the complex between the CRD of ERGIC-53 and MCFD2 was solved by molecular replacement and refined to 1.84 Å resolution (Fig. 1*A*). The CRD of ERGIC-53 assumes a β-sandwich fold consisting of two antiparallel β-sheets (β2, β5, β7, β8, β9, β10, β14, and β1, β6, β11, β12, β13, β15), two short β-strands (β3 and β4), and three 3_{10} helices, which is consistent with the previously reported crystal structure of rat ERGIC-53-CRD alone (13). The two crystal structures can be superposed with an average rms deviation of

Author contributions: M. Nishio, Y.K., S.W., H.S., S.U., M. Noda, A.R.M., and K.F. performed research; M. Nishio, Y.K., and K.Y. contributed new reagents/analytic tools; M. Nishio, Y.K., T.M., H.S., S.U., M. Noda, and A.R.M. analyzed data; M. Nishio, Y.K., T.M., S.W., S.U., H.-P.H., and K.K. wrote the paper; and Y.K. and K.K. designed research.

The authors declare no conflict of interest.

This article is a PNAS Direct Submission.

Data deposition: The atomic coordinates of the MCFD2/ERGIC-53-CRD complex have been deposited at the Protein Data Bank (PDB; www.rcsb.org) under accession code 3A4U.

[1]To whom correspondence should be addressed at: Okazaki Institute for Integrative Bioscience and Institute for Molecular Science, National Institutes of Natural Sciences, 5-1 Higashiyama, Myodaiji, Okazaki 444-8787, Japan, E-mail: kkatonmr@ims.ac.jp

This article contains supporting information online at www.pnas.org/cgi/content/full/0908526107/DCSupplemental.

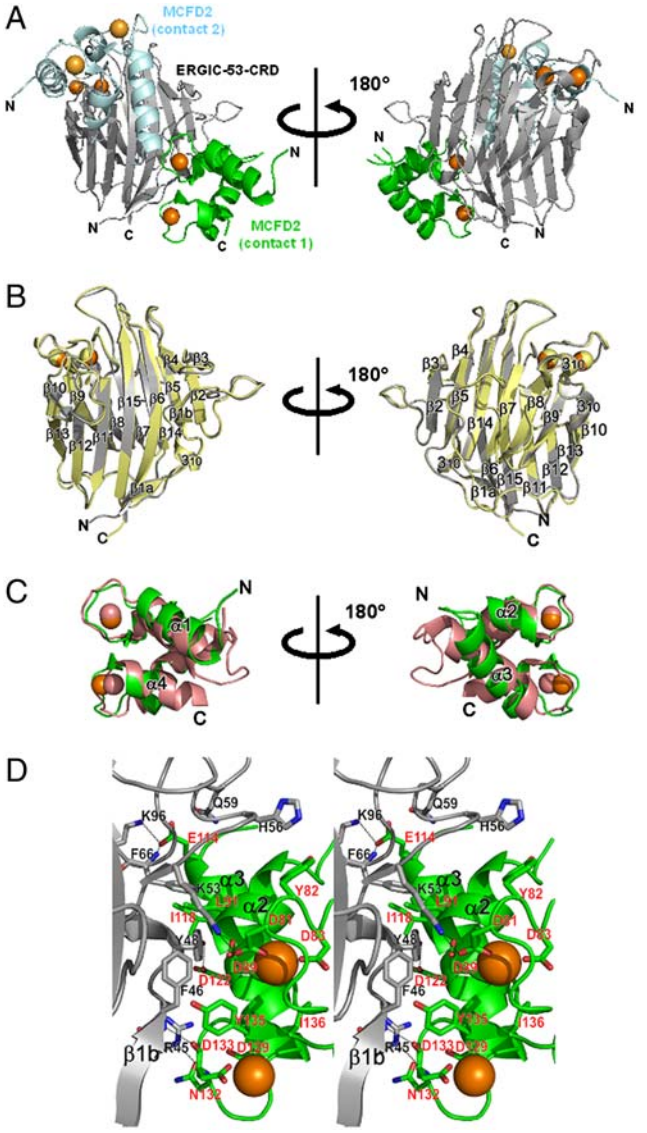

Fig. 1. Structure of the complex of MCFD2 and ERGIC-53-CRD. (*A*) Overall view of the complex. ERGIC-53-CRD is colored gray, whereas MCFD2 is colored green (at contact 1) and pale blue (at contact 2). (*B*) Superposition of human ERGIC-53-CRD complexed with MCFD2 (*Gray*) and uncomplexed rat ERGIC-53-CRD (*Yellow*). The orientation of human ERGIC-53-CRD is exactly the same as that shown in A and secondary structure elements are labeled. (*C*) Structural change of MCFD2 upon biding to ERGIC-53. Superposition of the ERGIC-53-CRD-bound (*Green*, present study) and uncomplexed [*Magenta*, the closest structure in the NMR ensemble deposited in PDB: Accession code 2VRG (16)] forms of MCFD2. The orientation of MCFD2 is exactly the same as that shown in A (contact 1) and secondary structure elements are labeled. (*D*) Close-up stereo view of the contact 1 interface between ERGIC-53-CRD (*Gray*) and MCFD2 (*Green*), showing intermolecular contacts. Hydrogen bonds are represented by dotted lines. The bound Ca^{2+} ions are shown as spheres (*Orange* in the MCFD2/ERGIC-53-CRD complex).

0.4 Å for the Cα atoms, indicating that MCFD2 binding causes no significant structural changes in the CRD of ERGIC-53 (Fig. 1*B*). Also, the positions of the two Ca^{2+}-coordination sites, which adjoin the putative sugar-binding site (Fig. S1), are almost identical between the two structures.

On the other hand, MCFD2 assumes a cluster of four α-helices (α1, α2, α3, and α4) in the C-terminal EF-hand region, whereas the N-terminal segment (residues 27–65), which is shown to be disordered in the NMR study of MCFD2 alone (17), also gave no interpretable electron density in the complex. In contrast to ERGIC-53-CRD, there exist significant conformational differences between the free and ERGIC-53-CRD-bound forms of MCFD2 (2.0 Å rmsd for Cα atoms even with the closest structure in the NMR ensemble) (Fig. 1*C*), although the α1 and α4 helices and the N-terminal portion of α2 helix superimpose well. The α3 helix in the complex is tilted close to the ERGIC-53-CRD by approximately 20°. In the free form of MCFD2, the residues 90–101 form the slightly bent α2 helix, which is followed by the flexible loop consisting of the residues from 102 to 112. In the complex, the residues 97 and 98 are unwound and the residues 99–111 are not visible in the electron density map. These results suggest that MCFD2 undergoes conformational changes upon binding to the CRD of ERGIC-53.

Interfaces Between ERGIC-53-CRD and MCFD2. In this crystal structure, two different packing interactions are observed between ERGIC-53-CRD and two MCFD2 molecules, one of which is from the next unit cell (Fig. 1*A*). One interaction mode (designated as contact 1) is mediated by α2, α3 and loops α1-β1, and α3-α4 of MCFD2; and β1a, β1b, β2, β5, β15, 3_{10}-1 and loop β1-β2 of ERGIC-53-CRD. The other mode (designate as contact 2) involves α1, α2, α3 and α4 of MCFD2; and 3_{10}-1, loop β10-β12 and loop β12-β13 of ERGIC-53-CRD. Both of the interacting sites are remote from the sugar-binding site of the CRD.

In contact 1, a total of 1,316 $Å^2$ of accessible surface area is buried. The intermolecular hydrogen bonds are formed by residues Asp83, Asp89, Glu114, Asp122, Asn132, and Asp133 of MCFD2, and Arg45, Phe46, Tyr48, Lys53, Gln59, Phe66, and Lys96 of ERGIC-53-CRD (Fig. 1*D*). On the other hand, a total of 1,072 $Å^2$ of accessible surface area is buried in contact 2, where MCFD2 binding is mediated by both hydrogen bonds and van der Waals contacts. Residues involved in the intermolecular formation of hydrogen bonds are Gln73, Thr98, Glu116, Asp128, Phe141, and Lys143 of MCFD2, and Phe198, Tyr199, Phe220, Asp223, and Lys224 of ERGIC-53-CRD (Fig. S2). The values of buried surface area and numbers of intermolecular hydrogen bonds suggest that contact 1 mediates the intermolecular interaction more tightly.

Stoichiometry of the Interaction in Solution. To examine whether both modes of interactions are realized in solution, the stoichiometry of the interaction between MCFD2 and ERGIC-53 was determined by analytical ultracentrifugation. Sedimentation coefficient (C(s)) distributions (Fig. 2*A*) from sedimentation velocity (SV) experiments at 20.0 °C indicate s-values of MCFD2 and ERGIC-53-CRD are 1.6 S and 2.5 S, respectively. No other peaks were detected. Correspondences of monomer molecular masses estimated from the C(s) distributions for MCFD2 and ERGIC-53-CRD to those calculated from amino acid sequences (13534 for MCFD2 and 28028 for ERGIC-53-CRD) indicates that they are monomeric below the concentration ranges studied (<200 μM for MCFD2 and <100 μM for ERGIC-53-CRD). In the mixed solution, the complex composed of MCFD2 and ERGIC-53-CRD exhibited a peak with 3.0 S under 20 μM condition (Fig. 2*A*) and 100 μM condition (Fig. S3*A*). The molecular mass estimated of this complex is 41,100, indicating a 1:1 stoichiometry of interactions between MCFD2 and ERGIC-53-CRD.

The hydrodynamic parameters of each protein and their complex estimated from SV analysis were compared with the calculated s-value, S_h, from the three-dimensional structures (Table S1). Obviously, the S_h, values of free MCFD2 and ERGIC-53-CRD agree with those ($S_{20,w}$) obtained experimentally. As for the complex between the ERGIC-53-CRD and MCFD2, the coincidence of $S_{20,w}$ with S_h computed under the assumption of one of the two modes of interactions confirms a 1:1 stoichiometry and further supports the possibility of the contact 1-mode of interaction in solution.

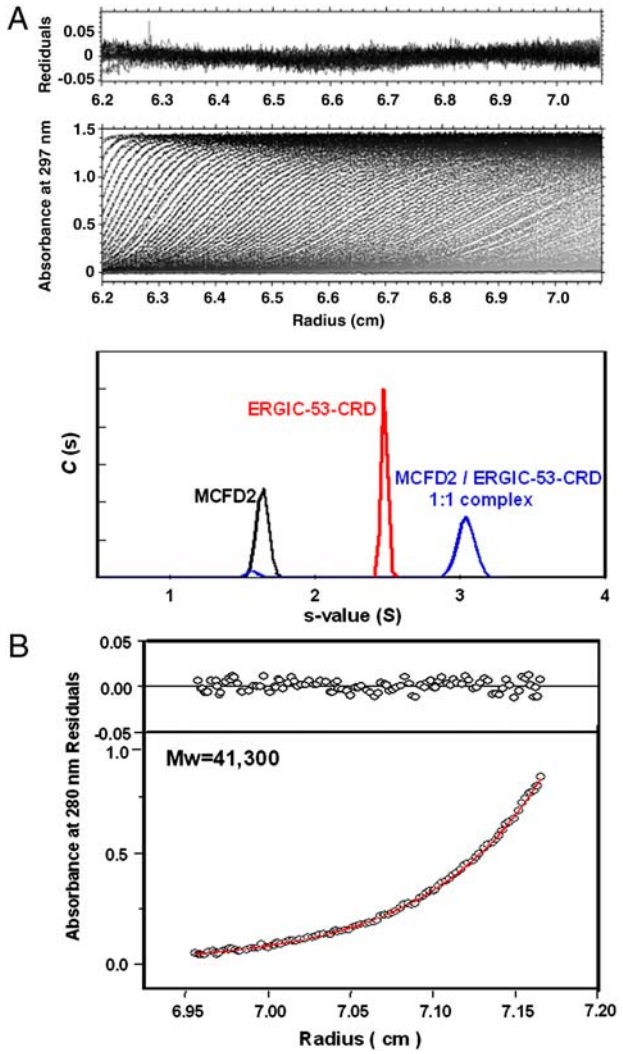

Fig. 2. Analytical ultracentrifugation of MCFD2, ERGIC-53-CRD, and their mixture. (*A*) SV experiments. (*Upper* and *Center*) Representative SV run at 60,000 rpm, result of *C*(s) distribution analysis of 20 μM solution of MCFD2 and ERGIC-53-CRD mixture with a 1:1 molar ratio, and the residual of the fit are shown. (*Lower*) Sedimentation coefficient distribution of the indicated protein that were obtained from the analysis of SV experiments. The uncomplexed ERGIC-53-CRD was not detected despite the fact that its molar extinction coefficient is larger than that of MCFD2. Therefore the MCFD2-ERGIC-53-CRD complex is stable and small peak at 1.6 S is not attributed to the dissociated form of MCFD2 from the complex but a small excess fraction of MCFD2 over ERGIC-53 under the experimental condition. (*B*) SE experiments. Representative equilibrium concentration gradient for 5 μM solution of MCFD2 and ERGIC-53-CRD mixture with 1:1 molar ratio. Best fit curve of nonlinear fitting employing single species model and the residual of the fit are shown.

In the sedimentation equilibrium (SE) experiment, nonlinear fitting of the equilibrium concentration gradient for the mixed solution (5 μM MCFD2 and 5 μM ERGIC-53-CRD) fit well with ideal single component model as judged from the uniform distribution of the residuals (Fig. 2*B*). Concentration gradients for mixed solution under different concentration conditions are also best fit with ideal single component model (Fig. S3*B* and *C*), although association-dissociation model was also assessed for the nonlinear fitting as our previous studies (18, 19). The molecular weight determined from the nonlinear fitting is 41,300. This value corresponds well to the molecular weight of a complex (41,562) composed of one MCFD2 and one ERGIC-53-CRD molecules. Hence, these SE results indicate the formation of stable 1:1 complex between MCFD2 and ERGIC-53-CRD, which is consistent with the result obtained from the SV experiment.

Interaction Analyses by NMR and Mutagenesis. To determine which of the two interaction modes observed in the crystal is actually exhibited in solution, we conducted NMR analyses by using ^{15}N-labeled MCFD2 and the synthetic peptides corresponding to the ERGIC-53 segments involved in contact 1 (Arg44-His56) and contact 2 (Ile 216-Tyr227). Upon titration with the contact 1 peptide, significant chemical shift changes were observed in the residues of MCFD2, especially those located in the EF-hand motifs and the loop connecting them, whereas the chemical shift perturbations induced with contact 2 peptide were much less pronounced (Fig. 3). The chemical shift perturbations with the contact 1 peptide were virtually abolished by the D89A mutation, which is located in the contact 1 interface of MCFD2 and associated with F5F8D (Fig. S4). These results suggest that the widespread chemical shift perturbations reflect the conformational change of MCFD2 upon binding to the contact 1 peptide, in accordance with the crystallographic data. Furthermore, ultracentrifugation and nanoflow electrosplay ionization mass spectrometric (nESI-MS) analyses revealed that the amino acid substitutions at the contact 1 interface, i.e. D122V in MCFD2 and R45A in ERGIC53-CRD, destabilize the complex whereas the point mutations introduced into the contact 2 interface, i.e. E116A and D128A in MCFD2 and Y199A and K224A in ERGIC-53-CRD, have no impact on their interaction (Figs. S5 and S6). On the basis of all these data, we conclude that MCFD2 and the CRD of ERGIC-53 form a 1:1 complex in solution through the contact 1-mode of interaction. The isothermal titration calorimetry (ITC) data showed that this interaction is not influenced by carbohydrate binding to ERGIC-53-CRD (Fig. S7).

Discussion

In the present study, we have determined the three-dimensional structure of the complex between MCFD2 and the CRD of ERGIC-53. In human, ERGIC-53 together with VIP36 and its homolog VIPL constitute a family of leguminous type lectins (20, 21). These proteins have different intracellular distributions and dynamics in the ER-Golgi system in the secretory pathway (22–25). Among these three lectins, only ERGIC-53 interacts with MCFD2 despite the structural similarities of their CRDs (3, 13, 15). Our structural data indicate that ERGIC-53 binds MCFD2 primarily through the segment spanning from β1a to β2 strands of the CRD. The amino acid residues located in this region are much less conserved between ERGIC-53 and VIP36/VIPL (Fig. S1*A*). In addition, comparison of the crystal structures of the CRDs demonstrates that the loops connecting β1b and β2 strands exhibit marked conformational differences between ERGIC-53 and VIP36 despite their overall structural similarities (Fig. S1*B*). These structural differences account for the specific binding of MCFD2 to ERGIC-53.

So far, seven missense mutations of *MCFD2* have been reported in F5F8D families (2, 9). These mutations cause amino acid substitutions in the first EF-hand motif (D81Y and D89A) and the second EF-hand motif (D122V, D129E, Y135N, and I136T/V). All the mutations except for Y135N have already been tested for in vitro and/or in vivo interactions with ERGIC-53 and shown to result in impaired binding (3, 10, 12, 17). The present study also confirmed the negative effects of these mutations on the binding capability to ERGIC-53-CRD (Figs. S4–S6). Our crystal structure revealed that, four of these amino acid residues, D81, D89, D122, and Y135 are directly involved in the intermolecular interaction with ERGIC-53, whereas the remaining two residues (D129 and I136) are involved in Ca^{2+}-coordination and therefore crucial for structural integrity of MCFD2 (Fig. 1*D*). A recently reported nonsense mutation of *MCFD2* results in deletion of the C-terminal three residues Ser144, Leu145, and Gln146. This truncated

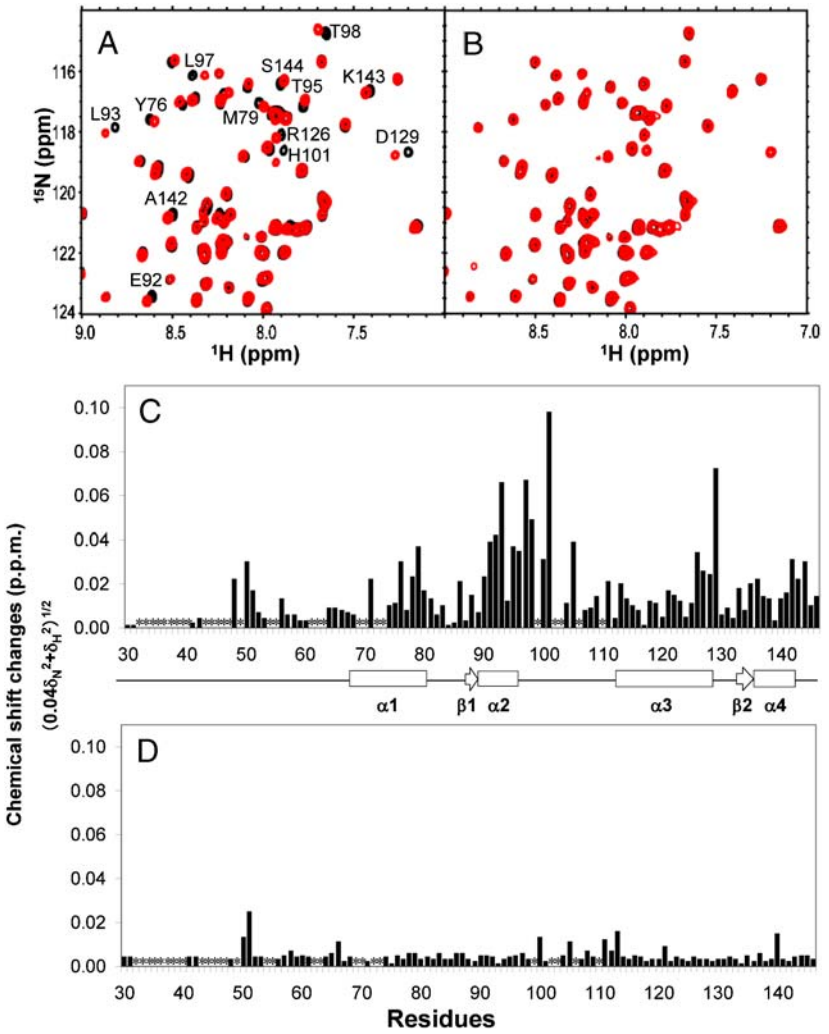

Fig. 3. NMR analysis of the interactions. ^{15}N-labeled MCFD2 was titrated with the synthetic peptides corresponding to the segments of ERGIC-53-CRD involved in contact 1 (*A* and *C*) and contact 2 (*B* and *D*) in the crystal structure. ^{1}H-^{15}N HSQC spectra (*A* and *B*) measured in the absence (*Black*) and presence (*Red*) of 5-fold molar excess of the peptides and plots of chemical shift perturbation data (*C* and *D*) obtained therefrom. Asterisk indicates residues whose chemical shift perturbation data could not be obtained due to severe broadening and/or peak overlapping.

MCFD2 mutant also exhibits impaired binding to ERGIC-53 (26). In the crystal structure, the C-terminal residues of MCFD2 gave no electron density but are obviously remote from the binding site for ERGIC-53-CRD. As shown by the previous CD data (26), the C-terminal residues are likely to confer structural integrity of MCFD2 and thereby contribute to the interaction with ERGIC-53 in an indirect manner.

Our present data also indicate that MCFD2 undergoes significant conformational alteration upon binding to the ERGIC-53, whereas MCFD2 binding has little impact on the conformation of ERGIC-53-CRD. In addition, the MCFD2 binding site is located remotely from the sugar-binding site on ERGIC-53-CRD (Fig. S1*B*). These observations suggest that sugar-binding affinity and specificity of ERGIC-53 are influenced neither directly nor allosterically by the interaction with MCFD2. Indeed, our ITC data indicate that the sugar-binding to ERGIC-53-CRD is independent of its interaction with MCFD2 (Fig. S7). In accordance with these results, ERGIC-53 has been shown to be able to bind cathepsin Z and cathepsin C as cargo glycoproteins in an MCFD2-independent fashion (11). This strongly implies that MCFD2 operates as a recruitment factor for FV and FVIII.

In many cases, EF-hand domains use their finger-motifs to form ligand-binding pockets on the opposite face of the Ca^{2+}-binding sites (27). MCFD2, however, does not adopt this typical mode of ligand-binding but uses the back of the EF-hand for the interaction with ERGIC-53-CRD, which results in the allosteric conformational change of the canonical ligand-binding site. Our structural data lead us to propose a model of functional coordination between ERGIC-53 and MCFD2. MCFD2 is converted into the active form upon complex formation with ERGIC-53 and thereby becomes able to capture polypeptide segments of FV and FVIII in cooperation with ERGIC-53 interacting with their carbohydrate moieties. These coagulation factors are heavily glycosylated and therefore bind the ERGIC-53 oligomer avidly in the ER but become released upon arrival to acidic postER compartments because the sugar-binding of ERGIC-53 is pH-dependent (28). Thus, this study provides new insights into the mechanisms underlying sorting and trafficking of the two coagulation factors mediated by the ERGIC-53/MCFD2 cargo receptor complex. Targeting the ERGIC-53/MCFD2 complex has been proposed as a therapeutic approach to anticoagulation (9). Considering our finding of a conformational change of MCFD2 upon complex formation with ERGIC-53, it appears that such an undertaking should focus on MCFD2.

Methods

Protein Expression. DNA fragments encoding MCFD2 were cloned into the pET-16b plasmid (N-terminal hexahistidine tag) and expressed in the

Escherichia coli BL21(DE3) codonplus strain induced with 0.5 mM isopropyl β-D-thiogalactopyranoside. For NMR analyses, the protein was expressed in M9 minimal medium with appropriate [^{15}N]NH_4Cl and/or [^{13}C]glucose. The protein purified by a Ni^{2+}-NTA high performance column (GE Healthcare), and subsequently by an anion exchange column (GE Healthcare) for crystallization. For ultracentrifuge, NMR, and nESI-MS analyses, the hexahistidine tag was cleaved by incubation with factor Xa (Novagen) and further purified by using anion exchange chromatography. The DNA fragment encoding residues 31-269, corresponding to the CRD of human ERGIC-53 was cloned into the pCold III plasmid and expressed in *E. coli* (BL21 (DE3)) as inclusion bodies, which were then solubilized by 6 M guanidinium chloride. The protein solution was diluted with a refolding buffer composed of 50 mM Tris-HCl, pH 8.0, 0.4 M L-arginine, 5 mM glutathione reduced form, and 0.5 mM glutathione oxidized form. The proteins were further purified using a Superdex 75 gel filtration column (GE Healthcare). Amino acid substitutions of MCFD2 and ERGIC-53-CRD were made by standard PCR and genetic engineering techniques. The mutated proteins were expressed and purified following the same protocol used for the wild-type proteins.

Crystallization, Data Collection, and Structure Determination. After mixing ERGIC-53-CRD and MCFD2, the fraction containing their complex was isolated by using a Superdex 75 gel filtration column (GE Healthcare) and then dialyzed against 10 mM Tris-HCl, pH 8.0, containing 100 mM $CaCl_2$. Crystals of the complex between MCFD2 and the CRD of ERGIC-53 were obtained at 16 °C by using the hanging-drop vapor diffusion method. The reservoir buffer contained 0.2 M sodium tartrate, pH 5.5, and 20% PEG 3,350. For cryoprotection, the crystals were soaked in the crystallization buffer containing 20% (v/v) glycerol and immediately frozen in the cryostream. Diffraction data were collected using synchrotron radiation beamline BL5A at Photon Factory, KEK. Data processing and reduction were carried out with the MOSFLM (29) and SCALA (30). There was one complex in the asymmetric unit.

The ERGIC-53-MCFD2 structure was solved by molecular replacement with the CRD domain of rat ERGIC-53 (PDB accession code 1R1Z) as a search model using the program MOLREP (31). An initial model was built using ARP/wARP (32). Manual building was carried out using the program COOT (33)and alternated with several cycles of refinement using the program REFMAC5 (34). The structure was refined to an R_{cryst} of 18.8% and an R_{free} of 20.0% for the data between 50 and 1.84 Å resolution. The final model contains residues 41–268 of the CRD of ERGIC-53 and residues 66–98 and 112–143 of MCFD2, four calcium ions, four glycerol molecules, and 189 solvent molecules. The electron densities of the first 39 N-terminal residues (27–65) and the C-terminal 3 residues (143–146) and the loop comprised of residues 99–111 of MCFD2 were not visible, suggesting that this region possesses a significant degree of flexibility. Stereochemistry of the final model was checked using the program PROCHECK (35), which indicated that 89.2% and 10.8% of the residues constituting ERGIC-53-CRD and MCFD2 were in the most favored and allowed regions of the Ramachandran plot, respectively. There are no residues in both the generously allowed and disallowed regions of the Ramachandran plot. Data collection and refinement statics are summarized in Table 1. Structure superpositions were performed using Dali-lite (36) and COOT. The program AREAIMOL (37) was used to calculate accessible surface areas. Molecular graphics were generated using PyMOL (http://pymol.sourceforge.net).

Coordinates and structure factors have been deposited at the Protein Data Bank (PDB; www.rcsb.org) under accession code 3A4U.

Analytical Ultracentrifugation. SV and SE experiments were performed in the buffer (10 mM MES, pH 6.0, 150 mM NaCl, and 100 mM $CaCl_2$) using Proteomelab XL-I Analytical Ultracentrifuge (Beckman–Coulter). In SV analysis, samples of MCFD2 (200 μM), ERGIC-53-CRD (20 μM and 100 μM), and their mixtures with a 1:1 molar ratio (20 μM and 100 μM) were measured. Runs were carried out at 60,000 rpm and at a temperature of 20.0 °C using 12 mm aluminum double sector centerpieces and four-hole An60 Ti analytical rotor equilibrated to 20.0 °C. The evolution of the resulting concentration gradient was monitored with absorbance detection optics at appropriate wavelength (281 nm and 297 nm) according to the concentration of the solution, where the absorbance of the solution becomes between 0.8 and 1.2. Rayleigh inference detection system was also employed. The radial increment was 0.003 cm and at least 150 scans were collected between 5.9 and 7.25 cm from the center of rotation axis. All SV raw data were analyzed by the continuous *C*(s) distribution model in the software program SEDFIT11.71 (38). The position of the meniscus and frictional ratio (f/f_0) were set to vary as fitted parameters and time-invariant noise and radian-invariant noise were removed. Additional parameter for the analysis included partial specific volumes calculated from the amino acid composition (MCFD2: 0.719 cm^3/g; ERGIC-53-CRD: 0.724 cm^3/g; MCFD2/ERGIC-53-CRD complex: 0.722 cm^3/g), and buffer density ($\rho = 1.0139$ g/cm^3) and viscosity ($\eta = 1.0376$ centipoises) calculated using the program UltraScanII version 9.9 (http://www.ultrascan.uthscsa.edu/) (37). A resolution of 300 increments between 0.5 and 10 S were entered and maximum entropy regularization was used ($p = 0.68$). The absence of concentration dependent interactions were verified and ideal sedimentation behavior was confirmed by obtaining molar mass estimates from *C*(s) close to the values calculated from the amino acid sequences. Calculation of hydrodynamic parameters including s-value were carried out using three-dimensional structures of each protein or protein complex by using the program US-SOMO implemented in UltraScanII version 9.9 (39, 40). Molar extinction coefficient spectra of MCFD2 (ex. 5120 mol^{-1} cm^2 at 280 nm) and ERGIC-53-CRD (ex. 38810 mol^{-1} cm^2 at 280 nm) were derived using the program Sednterp version 1.09. For evaluation of the effects of the point mutations, equi-molar mixtures (5 μM each) of the wild-type or mutated versions of ERGIC-53-CRD and MCFD2 were subjected to the SV analysis.

In SE analysis, samples of MCFD2 and ERGIC-53 mixtures with a 1:1 molar ratio (5 μM, 10 μM, and 100 μM) were centrifuged at 20,000 rpm and at 20.0 °C using 12 mm charcoal-epon double sector centerpieces using four-hole An60 Ti analytical rotor. Absorbance detection optics and Rayleigh interference detection system were used for the concentration gradient observation. Equilibrium was confirmed by the complete overlapping of two different concentration gradients obtained at 6 h interval. Nonlinear least squares fitting of the equilibrium concentration gradients were performed by the programs Origin6.0 (OriginLab Corporation) and SigmaPlot11 (Systat Software Inc) using the single fitting and global fitting modes.

NMR Analyses. Proteins were dissolved in 10 mM Tris-HCl, pH 7.5, containing 100 mM $CaCl_2$, 2.4 mM NaN_3, and 10% (v/v) D_2O. All NMR spectra were acquired at 303 K using Avance600 (Bruker BioSpin) and ECA920 (JEOL) spectrometers. Although the backbone resonances of MCFD2 have been deposited in the Biological Magnetic Resonance Bank under accession code BMRB-15789 (18), these data were collected at a different buffer condition from this report. Therefore, we assigned the backbone resonances of MCFD2 as well. The chemical shifts of MCFD2 were assigned using the following experiments: 2D ^{1}H-^{15}N HSQC, 3D HNCA, HN(CO)CA, HNCO, HN(CA)CO, CBCA (CO)NH and HNCACB spectra. To observe chemical shift perturbation, 5-fold molar equivalents of the synthetic peptides, which are corresponding to the

Table 1. Data collection and refinement statics

Crystallographic data	
Space group	$P3_121$
Unit cell	
a/b/c (Å)	59.4 59.4 198.8
α/β/γ (°)	90.00 90.00 120.00
Data processing statistics	
Beam line	PF-BL5A
Wavelength (Å)	1.000
Resolution (Å)	49.8 – 1.84 (1.94 – 1.84)*
Total reflections	247663
Unique reflections	36530
Redundancy	6.8 (7.0)
Completeness (%)	99.9 (100.0)
Rmerge (%)	5.9 (25.7)
$I/\sigma(I)$	19.5 (6.1)
Refinement statistics	
Resolution (Å)	49.81 – 1.84
Rwork (%)	18.8
Rfree (%)	20.0
Rmsd from ideal values	
Bond length (Å)	0.007
Angle (°)	1.086
Ramachandran plot (%)	
Most favored	89.2
Additionally allowed	10.8
Generously allowed	0.0
Disallowed	0.0
Number of molecules and atoms	
Protein atoms	2315
Ca^{2+} ions	4
Glycerol	4
Water molecules	189

*Values in parentheses are for the highest resolution shell.

ERGIC-53-CRD segments Arg44-His56 (RRFEYKYSFKGPH) and Ile216-Tyr227 (INNGFTPDKNDY) (purchased from AnyGen), were individually added to wild-type or mutated [^{15}N]MCFD2 solutions. The chemical shift perturbation data were estimated for each residue using the equation $(0.04\delta_N^2 + \delta_H^2)^{1/2}$ (ppm), where δ_N and δ_H represent the change in nitrogen and proton chemical shift upon mixing of MCFD2 and the peptides, respectively.

Mass spectrometry. Protein mixtures composed of wild-type or mutated MCFD2 and ERGIC-53-CRD (25 μM each) were subjected to mini gel filtration columns (BioRad) equilibrated with 250 mM ammonium acetate (pH 6.0) for buffer exchange. Spectral data of ions generated by nanoflow electrospray ionization were acquired on an Synapt HDMS mass spectrometer (Waters) modified for high mass operation (41). Nanospray ionization was performed using gold-coated glass capillaries prepared in-house. Typical conditions included 2–3 μL of aqueous protein solution, capillary voltage of 1.1–1.7 kV, cone voltage of 80–120 V, trap and transfer collision energy voltages of 30 and 10 V respectively, except during MS/MS dissociation when the trap collision energy voltage was increased to 100 V. The source pressure was maintained at 2×10^{-2} mbar. Spectra were calibrated externally using an aqueous 33 mg/mL^{-1} solution of cesium chloride.

Calorimetric Analysis. ITC experiments were performed using an iTC$_{200}$ calorimeter (GE healthcare UK Ltd.). Manα1-2Man (Sigma–Aldrich) or the M8.1 isomer of $Man_8GlcNAc_2$-PA (16) were used as carbohydrate ligands.

ACKNOWLEDGMENTS. We thank Michiko Nakano (Institute for Molecular Science) for her help in NMR measurements. We thank Kiyomi Senda (Nagoy City University) and Yukiko Isono (Okazaki Institute for Integrative Bioscience) for their technical assistance in sample preparation. We thank Drs. Eiji Kurimoto (Meijo University), Norio Kudo (KEK), and Tatsuo Hikage (Nagoya University) for their supports in the data collection at the early stage of this study. This work was supported by Grant-in-Aid for Scientific Research on Priority Area 20059030, Grant-in-Aid for Scientific Research on Innovative Areas 20107004, Grant-in-Aid for Scientific Research (B) 21370050, Grant-in-Aid for Young Scientists (Start-up) 21870052, and Nanotechnology Support Project from the Ministry of Education, Culture, Sports, Science, and Technology and by CREST project from the Japan Science and Technology Agency.

1. Oeri J, Matter M, Isenschmid H, Hauser F, Koller F (1954) [Congenital factor V deficiency (parahemophilia) with true hemophilia in two brothers.]. *Bibl Paediatr* 58:575–88.
2. Zhang B (2009) Recent developments in the understanding of the combined deficiency of FV and FVIII. *Br J Haematol* 145:15–23.
3. Zhang B, et al. (2008) Genotype-phenotype correlation in combined deficiency of factor V and factor VIII. *Blood* 111:5592–600.
4. Zhang B, et al. (2006) Combined deficiency of factor V and factor VIII is due to mutations in either LMAN1 or MCFD2. *Blood* 107:1903–7.
5. Schweizer A, Fransen JA, Bachi T, Ginsel L, Hauri HP (1988) Identification, by a monoclonal antibody, of a 53-kD protein associated with a tubulo-vesicular compartment at the cis-side of the Golgi apparatus. *J Cell Biol* 107:1643–53.
6. Kamiya Y, et al. (2008) Molecular basis of sugar recognition by the human L-type lectins ERGIC-53, VIPL, and VIP36. *J Biol Chem* 283:1857–61.
7. Appenzeller C, Andersson H, Kappeler F, Hauri HP (1999) The lectin ERGIC-53 is a cargo transport receptor for glycoproteins. *Nat Cell Biol* 1:330–4.
8. Lahtinen U, Svensson K, Pettersson RF (1999) Mapping of structural determinants for the oligomerization of p58, a lectin-like protein of the intermediate compartment and cis-Golgi. *Eur J Biochem* 260:392–7.
9. Zhang B, et al. (2003) Bleeding due to disruption of a cargo-specific ER-to-Golgi transport complex. *Nat Genet* 34:220–5.
10. Kawasaki N, et al. (2008) The sugar-binding ability of ERGIC-53 is enhanced by its interaction with MCFD2. *Blood* 111:1972–9.
11. Nyfeler B, Zhang B, Ginsburg D, Kaufman RJ, Hauri HP (2006) Cargo selectivity of the ERGIC-53/MCFD2 transport receptor complex. *Traffic* 7:1473–81.
12. Zhang B, Kaufman RJ, Ginsburg D (2005) LMAN1 and MCFD2 form a cargo receptor complex and interact with coagulation factor VIII in the early secretory pathway. *J Biol Chem* 280:25881–6.
13. Velloso LM, Svensson K, Schneider G, Pettersson RF, Lindqvist Y (2002) Crystal structure of the carbohydrate recognition domain of p58/ERGIC-53, a protein involved in glycoprotein export from the endoplasmic reticulum. *J Biol Chem* 277:15979–84.
14. Velloso LM, Svensson K, Pettersson RF, Lindqvist Y The crystal structure of the carbohydrate-recognition domain of the glycoprotein sorting receptor p58/ERGIC-53 reveals an unpredicted metal-binding site and conformational changes associated with calcium ion binding. *J Mol Biol* 334:845–51.
15. Satoh T, et al. (2007) Structural basis for recognition of high mannose type glycoproteins by mammalian transport lectin VIP36. *J Biol Chem* 282:28246–55.
16. Kamiya Y, et al. (2005) Sugar-binding properties of VIP36, an intracellular animal lectin operating as a cargo receptor. *J Biol Chem* 280:37178–82.
17. Guy JE, Wigren E, Svard M, Hard T, Lindqvist Y (2008) New insights into multiple coagulation factor deficiency from the solution structure of human MCFD2. *J Mol Biol* 381:941–55.
18. Kato K, et al. (2000) Structural basis of the interaction between IgG and Fcγreceptors. *J Mol Biol* 295:213–24.
19. Oda M, et al. (2006) Regional and segmental flexibility of antibodies in interaction with antigens of different size. *Febs J* 273:1476–87.
20. Kato K, Kamiya Y (2007) Structural views of glycoprotein-fate determination in cells. *Glycobiology* 17:1031–44.
21. Kamiya Y, Kamiya D, Urade R, Suzuki T, Kato K (2009) Sophisticated modes of sugar recognition by intracellular lectins involved in quality control of glycoproteins. *Glycobiology Research Trends*, ed Powell G (NOVA Science Publishers, New York), pp 27–40.
22. Füllekrug J, Scheiffele P, Simons K (1999) VIP36 localisation to the early secretory pathway. *J Cell Sci* 112(Pt 17):2813–21.
23. Hauri HP, Kappeler F, Andersson H, Appenzeller C (2000) ERGIC-53 and traffic in the secretory pathway. *J Cell Sci* 113 (Pt 4):587–96.
24. Neve EP, Svensson K, Fuxe J, Pettersson RF (2003) VIPL, a VIP36-like membrane protein with a putative function in the export of glycoproteins from the endoplasmic reticulum. *Exp Cell Res* 288:70–83.
25. Nufer O, Mitrovic S, Hauri HP (2003) Profile-based data base scanning for animal L-type lectins and characterization of VIPL, a novel VIP36-like endoplasmic reticulum protein. *J Biol Chem* 278:15886–96.
26. Nyfeler B, et al. (2008) Deletion of 3 residues from the C-terminus of MCFD2 affects binding to ERGIC-53 and causes combined factor V and factor VIII deficiency. *Blood* 111:1299–301.
27. Gifford JL, Walsh MP, Vogel HJ (2007) Structures and metal-ion-binding properties of the Ca^2+-binding helix-loop-helix EF-hand motifs. *Biochem J* 405:199–221.
28. Appenzeller-Herzog C, Roche AC, Nufer O, Hauri HP (2004) pH-induced conversion of the transport lectin ERGIC-53 triggers glycoprotein release. *J Biol Chem* 279:12943–50.
29. Leslie AG (1999) Integration of macromolecular diffraction data. *Acta Crystallogr D Biol Crystallogr* 55:1696–702.
30. Collaborative Computational Project 4 . *Acta Crystallogr D Biol Crystallogr* 50:760–763.
31. Vagin A, Teplyakov A (1997) MOLREP: An Automated Program for Molecular Replacement. *J Appl Crystallogr* 30:1022–1025.
32. Morris RJ, Perrakis A, Lamzin VS (2003) ARP/wARP and automatic interpretation of protein electron density maps. *Methods Enzymol* 374:229–44.
33. Emsley P, Cowtan K (2004) Coot: Model-building tools for molecular graphics. *Acta Crystallogr D Biol Crystallogr* 60:2126–32.
34. Murshudov GN, Vagin AA, Dodson EJ (1997) Refinement of macromolecular structures by the maximum-likelihood method. *Acta Crystallogr D Biol Crystallogr* 53:240–55.
35. Laskowski RA, MacArthur MW, Moss DS, Thornton JM (1993) PROCHECK: A program to check the stereochemical quality of protein structures. *J Appl Crystallogr* 26:283–291.
36. Holm L, Park J (2000) DaliLite workbench for protein structure comparison. *Bioinformatics* 16:566–7.
37. Saff EB, Kujilaars ABJ (1997) Distributing many points on a sphere. *Math Intell* 19:5–11.
38. Schuck P (2000) Size-distribution analysis of macromolecules by sedimentation velocity ultracentrifugation and lamm equation modeling. *Biophys J* 78:1606–19.
39. Demeler B (2005) *In Modern Analytical Ultracentrifugation: Techniques and Methods*, ed Scott DJ (Royal Society of Chemistry, UK), pp 210–229.
40. Brookes E, Demeler B, Rosano C, Rocco M (2010) The implementation of SOMO (SOlution MOdeller) in the UltraScan analytical ultracentrifugation data analysis suite: Enhanced capabilities allow the reliable hydrodynamic modeling of virtually any kind of biomacromolecule. *Eur Biophys J* 39:423–435.
41. Sobott F, Hernandez H, McCammon MG, Tito MA, Robinson CV (2002) A tandem mass spectrometer for improved transmission and analysis of large macromolecular assemblies. *Anal Chem* 74:1402–7.